

Co-Ni CARBONATE HYDROXIDE NANONEEDLES SELF-SUPPORTED ON Ni FOAM AS A BIFUNCTIONAL CATALYST FOR OVERALL WATER SPLITTING

X. L. WANG^a, W. FENG^{a,b}, X. G. AN^a, C. LU^a, W. J. BAI^a, F. Y. SUN^a,
Q. Q. KONG^{a,b*}

^a*School of Mechanical Engineering, Chengdu University, Chengdu 610106, Sichuan, PR China*

^b*College of Architecture and Environment, Sichuan University, Chengdu 610065, PR China*

High performance non-noble bi-functional electrocatalysts are highly demanded towards low-cost water splitting. Herein, Co-Ni carbonate hydroxide nanoneedles self-supported on Ni foam were prepared by a facile hydrothermal method. When it is assembled as the cathode and the anode in a two-electrode configuration, the combined cell demonstrates excellent catalysis performance, with a current density of 10 mA cm⁻² at 1.62 V, due to the one-dimensional shape and hybrid amorphous/crystalline structure of Co-Ni carbonate hydroxide.

(Received June 15, 2020; Accepted November 30, 2020)

Keywords: Overall water splitting, Alkaline solution, Co-Ni carbonate hydroxide, Hydrothermal method

1. Introduction

Low-cost and green production of hydrogen (H₂) is critical for hydrogen economy, which has been extensively studied in the past decades^[1-3]. One promising approach is to produce H₂ from water splitting, including hydrogen evolution reaction (HER) and oxygen evolution reaction (OER). However, these reactions are kinetically sluggish and require high-performance electrocatalysts to reduce the overpotential^[4, 5]. So far, platinum^[6], sulfides^[7], oxides^[8], phosphide^[9, 10], carbide^[11] and selenide^[12] have been developed as promising catalysts for HER. With respect to HER, OER is more complicated and the correlations between different elementary reactions often limit the reaction rate^[13-15]. As a result, only very limited noble metals, such as iridium (Ir) and ruthenium (Ru) and their compounds, can offer fast kinetics^[16-19]. Under this context, low-cost catalysts with high-performance for HER and OER are highly targeted towards efficient water splitting.

Recently, bi-functional electrocatalysts, which can catalyze HER and OER simultaneously, have been developed as a new approach for water splitting^[20-22]. Among various candidates, metal (oxy)hydroxide is particularly attractive due to its high performance and low cost^[23-25]. Coral-like FeNi(OH)_x can be conducted as a bi-functional electrocatalyst for overall water splitting in alkaline media^[26]. Coral structure makes the electrode surface much rougher and provides more active sites. NiFe-hydroxide nanoflake arrays supported on Ni foam (NF) also show high activity and excellent durability simultaneously, making it very attractive for practical use^[27]. The well-aligned nanoflake arrays with vertical orientation allow for full contact between active sites and electrolyte, and promote mass transfer and bubble release. For these catalysts, the performance often highly relies on the catalyst morphology, which is essentially determined by both surface reactivity and catalyst conductivity^[28].

Moreover, metal hydroxide incorporated with carbonate have been found have superior activity in water electrolysis. Wei et al reported cobalt carbonate hydroxide (CCH)

*Corresponding author: kongqingquan@163.com

supported on carbon black can offer a small overpotential of 0.509 V at a current density of 10 mA cm⁻² for OER in 0.1 M KOH^[29]. When take NF as support materials, CCH nanowire array show superior in activity and durability for OER under near neutral conditions, capable of driving 10 mA cm⁻² at an overpotential of only 332 mV^[30]. Although considerable recent progress has been made in developing metal carbonate hydroxide as OER catalysts in both alkaline and near-neutral media^[29-31], there have still been no reports on metal hydroxyl carbonate hydrate as bi-functional electrocatalyst for electrochemical overall water splitting.

In the present study, we have prepared one dimensional (1D) Co-Ni carbonate hydroxide (CNCH) nanoneedles on conductive NF substrate and investigated electrochemical overall water splitting for the first time. As demonstrated below, such hybrid structure has been identified as an excellent bi-functional electrocatalyst for overall alkaline water splitting for first time, achieving 10 mA cm⁻² at a cell voltage of 1.62 V.

2. Experimental part

2.1. Materials

All chemicals with analytical grade were purchased from Kelong. Ni foam was purchased from Kunshan Electronic Ltd, China.

2.2. Preparation of CNCH nanoneedles self-supported on Ni foam

Specifically, 2 mM Co(NO₃)₂·6H₂O, 10 mM urea and 2 mM NH₄F were thoroughly dissolved in 36 ml distilled (DI) water after 10 minutes magnetic stirring. Then the homogeneous solution was transferred to a 50 mL Teflon autoclaves. Ni foam (about 1×3 cm) was carefully cleaned with 3 M HCl solution and distilled water, and then ultrasonicated for 5 min to remove the NiO surface layer. Then cleaned Ni foam was immersed in the above mixture solution. The autoclaves were sealed for a hydrothermal reaction at 120 °C and 160 °C for 12 h (Abbreviated as CNCH-12/NF and CNCH-16/NF, respectively). Then the autoclaves were cooled down to room temperature. The as-prepared samples were carefully washed with deionized water and ethanol, respectively. After that, the samples were dried in a vacuum oven at 60 °C for 12h.

2.3. Characterizations

The morphologies of samples were observed with a field-emission scanning electron microscope (FESEM, FEI Inspect F50) and a High Resolution Transmission Electron Microscope (HRTEM, FEI Tecnai G2 F20 S-TWIN). X-ray diffraction patterns were recorded by an X-ray diffractometer (XRD, DX-2700B) with Cu K α radiation. X-ray photoelectronic spectroscopy (XPS) was recorded using an ESCALAB Model 250 spectrometer using an Al K α source (1486.6 eV). All the electrochemical investigations were carried out by a CHI660E electrochemical workstation (CH Instruments, China) in a standard three-electrode system controlled with a Pt plate electrode as a counter electrode, a saturated calomel electrode (SCE) as a reference electrode and prepared samples were used as the working electrode. The size of working electrode was restricted to 0.25 cm² to minimize the interference caused by the formation of gaseous products. Linear sweep voltammetry (LSV) and cyclic voltammetry (CV) were carried out in 1.0 M KOH solution.

2.4. Electrochemical measurements

All potentials measured were calibrated to RHE using the following equation: $E(\text{RHE}) = E(\text{SCE}) + 0.241 \text{ V} + 0.059 \cdot \text{pH}$. No iR compensation was applied in our testing data. Electrochemical impedance spectroscopy (EIS) was carried out from 10 kHz to 0.01 Hz with an amplitude of 5 mV.

3. Results and discussion

The CNCH nanoneedles were successfully grown on Ni foam through a facile hydrothermal method. The samples treated at 120 and 160 °C, labelled as CNCH-12/NF and CNCH-16/NF, have been employed below. The morphology of our samples were characterized by field-emission scanning electron microscope (FESEM). As shown in Fig. 1a-c, it is clearly indicated that Ni foam is uniformly covered by CNCH nanoneedles. TEM image in Fig. 1d further confirmed the nanoneedles structure of CNCH. These unique microstructures provide abundant active sites and easy-to-access paths for mass transfer, which is helpful to achieve high catalytic performance. High-resolution TEM image of the nanoneedle presented in Fig. 1e reveals that many amorphous regions can be observed (highlighted by white circles). XRD pattern shown in Fig. 2 exhibits that no new diffraction peaks can be detected except for three peaks of Ni, indicating the poor crystalline nature of CNCH nanoneedles, which coincides well with HRTEM results. The energy dispersive X-ray spectroscopy (EDX) elemental mapping (Fig. 1f) also indicates the homogeneous distribution of Co, Ni and O elements over the examined detection range at the surface of the CNCH nanoneedles. It is interesting to note that, Ni element were introduced by NF substrate during hydrothermal process without additional added of Ni salt (as will be confirmed by the following XPS analysis).

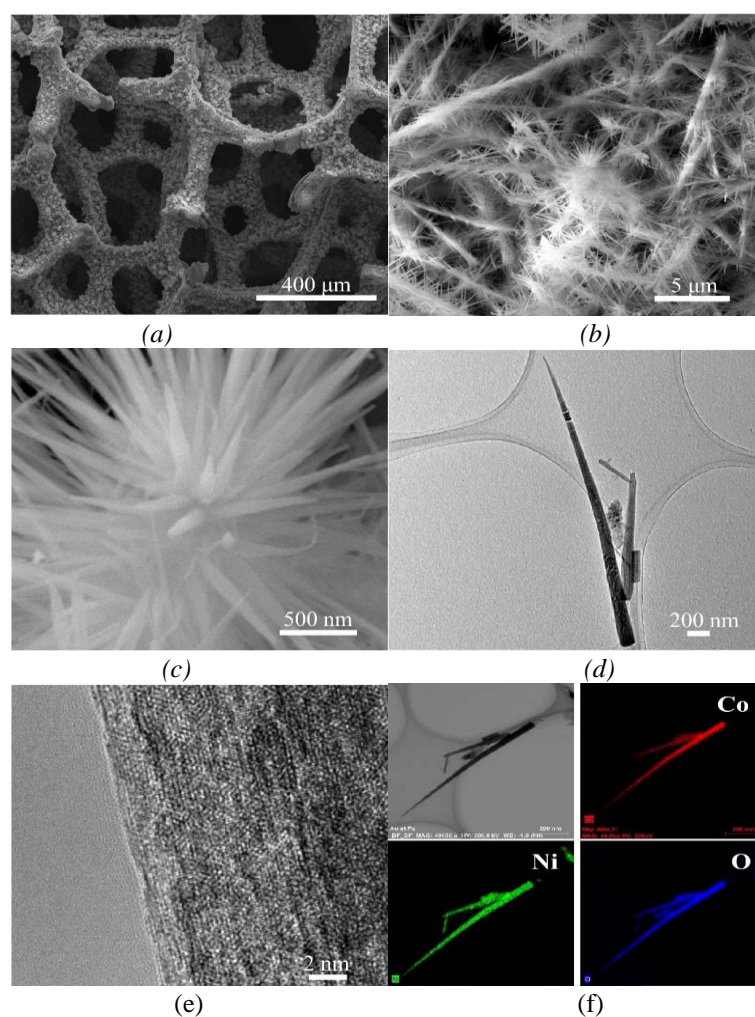


Fig. 1. (a, b, c) FESEM images of CNCH-12/NF. (d, e) TEM and HRTEM images of CNCH-12/NF. (f) EDX elemental mapping images of CNCH-12/NF.

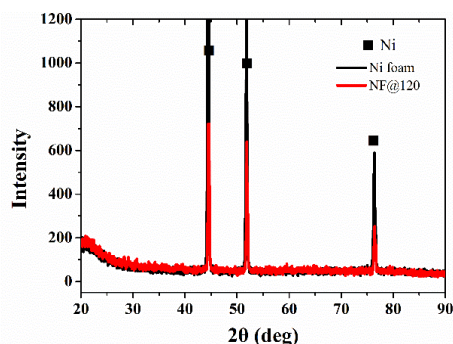


Fig. 2. XRD patterns of Ni foam and CNCH-12/NF.

X-ray photoelectron spectroscopy (XPS) was utilized to further investigate the chemical states of CNCH-12/NF. The survey spectrums clearly illustrate the presence of Co, Ni and O (Fig. 3a). The inset in Fig. 3a show the peak at 289 eV results from $-\text{C}(\text{O})\text{O}-$ group^[30]. From Fig. 3b, the characteristic peaks at 797.2 and 781.7 eV binding energies are identified as Co^{2+} species, whereas the other two peaks at 796.1 and 780.1 eV correspond to Co^{3+} species^[32]. As shown in Fig. 3c, the high-resolution XPS spectrum of Ni 2p shows two main peaks located at 855.3 and 873.0 eV with shakeup satellites at 880.0 and 862.2 eV, corresponding to Ni^{2+} (Ni 2p_{3/2} and Ni 2p_{1/2}, respectively), while the peaks at 875.0 and 856.7 eV are corresponded to Ni^{3+} ^[33]. Both Co 2p and Ni 2p XPS spectra indicate that the coexistence of $\text{Co}^{2+}/\text{Co}^{3+}$ and $\text{Ni}^{2+}/\text{Ni}^{3+}$. The O 1s spectrum was also fitted, confirming the presence of two oxygen species, OH^- groups of hydroxides (530.6 eV) and defect sites with low oxygen coordination (531.8 eV)^[27]. Combined with microstructure observation and XPS analysis, we can conclude that CNCH nanoneedles supported on Ni foam have been prepared.

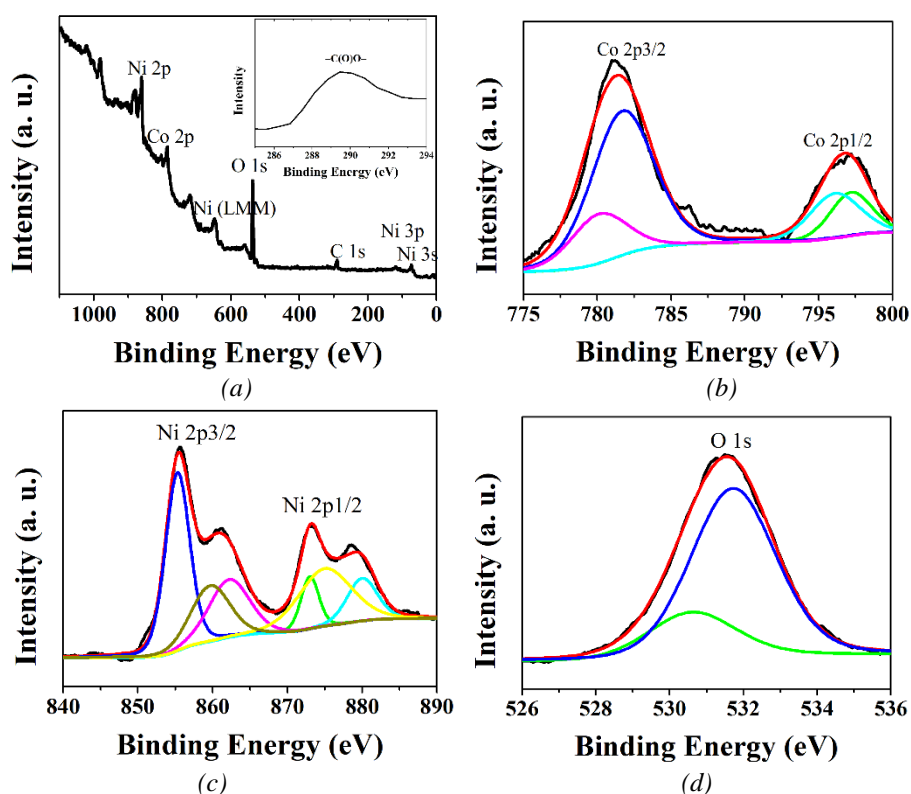


Fig. 3. (a) XPS total spectrum of CNCH-12/NF, XPS spectra of CNCH-12/NF in the (b) Co 2p, (c) Ni 2p, and (d) O 1s regions.

The electrocatalytic HER performance of Ni foam, CNCH-12/NF and CNCH-16/NF was evaluated in 1 M KOH with a standard three-electrode system. Fig. 4a shows the linear sweep voltammetry (LSV) curves without iR compensation. CNCH-12/NF exhibits the best catalytic, which demands an overpotential of 171 mV to reach a current density of 10 mA/cm². Tafel slopes were measured to further assess the catalytic performance. According to the mechanism of hydrogen evolution, there are three typical steps for HER, such as Discharge step (Volmer reaction), Desorption step (Heyrovsky reaction) and Recombination step (Tafel reaction)^[34]. Volmer reaction, Heyrovsky reaction, and Tafel reaction deliver typical Tafel slopes of 120, 40, and 30 mV/dec, respectively. As shown in Fig. 4b, the observed Tafel slope of CNCH-12/NF is 70 mV/dec, suggesting that the Volmer-Heyrovsky mechanism dominates HER process and the desorption step is the rate-determining step^[35, 36]. After 2000 cyclic voltammetry scanning, the LSV curves of CNCH-12/NF show no obvious changes (Fig. 5a), suggesting that the catalyst presents a long-term electrochemical stability for HER.

The electrocatalytic OER performance was also evaluated. Fig. 4c shows the LSV curves without iR compensation. CNCH-12/NF exhibits the best catalytic, which affords a current density of 50 mA/cm² with a relatively low overpotential of 368 mV. An oxidation peak around 1.3~1.4V was observed for both CNCH-12/NF and CNCH-16/NF. The oxidation peak at around 1.3V vs. RHE can be attributed to the oxidation of Co³⁺ to Co⁴⁺^[8, 37]. The anodic peak near 1.36 V vs. RHE was due to the change of Ni oxidation state from Ni²⁺ to Ni³⁺^[38]. Therefore, we can ascribe the oxidation peak of CNCH-12/NF and CNCH-16/NF to the oxidation state change of both Ni and Co ions. It should be noted that the oxidation peak of CNCH-12/NF is larger than CNCH-16/NF, indicating that more active materials were grown on the Ni foam when a proper hydrothermal temperature is employed. The higher Ni oxidation peak and lower onset potential suggest an easier redox transformation of Ni²⁺ to Ni³⁺, which is beneficial for OER^[39]. Tafel slopes were also analyzed and illustrated in Fig. 4d. The observed Tafel slope for CNCH-12/NF is 86 mV/dec, suggesting the outstanding catalytic kinetics on CNCH-12/NF. LSV curves after continuous CV cycles are shown in Fig. 5b, which shows a negligible decay after 2000 cycles.

Based on the measured HER and OER data, it appears that the prepared materials are promising candidates to build bi-functional electrode for full water splitting. We constructed a two-electrode configuration by employing CNCH-12/NF as both anode and cathode to explore water splitting in 1M KOH solutions. As shown in Fig. 4e, CNCH-12/NF||CNCH-12/NF affords a current density of 10 mA cm⁻² at a cell voltage of 1.62 V. In contrast, bare Ni foam requires higher cell voltages of 1.80 V to reach current densities of 10 mA cm⁻²^[40] under the same condition. The performance at the current density of 10 mA cm⁻² is also comparable or even better than most previously reported non-noble metal bi-functional catalysts for overall alkaline water splitting, e.g., CoNi(OH)_x||NiNx nanotube (~1.65V)^[30], NiCo-LDH/NF (1.66 V)^[41], NiO NRs-m-Ov (~1.64 V in 6M KOH)^[42], and porous CoP-based films with phase separation structure (1.65 V)^[43]. As shown in Fig. 4f, The CNCH-12/NF||CNCH-12/NF can maintain a current density of 10 mA cm⁻² for at least 10 h only with small increase of potential (<0.03 V), indicating an outstanding stability.

To further understand the enhanced catalytic activity of CNCH-12/NF, the electrochemically active surface areas were measured by the double-layer capacitance (C_{dl}) method in O₂ saturated 1 M KOH^[44]. CNCH-12/NF shows the highest C_{dl} of 10 mFcm⁻², indicating the abundant active sites for electrocatalysis. The interfacial reactions and electron-transfer kinetics were also evaluated by perform electrochemical impedance spectroscopy (EIS) from 10 kHz to 0.01 Hz with an amplitude of 5 mV. The experimental data were simulated by an electrical equivalent circuit composed of two constant phase elements (CPE)/resistive elements in series (inset in Fig. 6b). R1 is the ohmic resistance of the electrolyte and electrode. R2 and R3 are the charge transfer resistances. R3 of CNCH-12/NF is the smallest, indicating a faster charge transfer process for the electrocatalysis^[45]. The unique 1D nanoneedles structure of CNCH self-supported on Ni foam offers fast charge transport and direct electrical contact to the underlying current collector (see the inset image

in Fig. 6a). Early studies demonstrated that amorphous layers can provide much more active sites for electrocatalysis^[46]; therefore, high performance observed from the hybrid amorphous/crystalline structure presented in this work should originate from surface defects associated with amorphous structures (see Fig. 3d), which often act as active sites for electrocatalytic decomposition of water^[47]. While amorphous structure may be easily changed due to poor thermal instability and reconstruction under electrochemical conditions. As illustrated by TEM images in Fig. 7, fine lattice fringes can be clearly observed (Fig. 7b), indicating the existence of crystalline structures, which is different from the as-prepared sample. EDX mapping listed in Fig. 8 indicates that the distribution of Co, Ni and O elements has no change after the electrochemical measurement. Ren et al pointed out that amorphous film may evolve into porous interwoven nanorod arrays after OER testing, which brings more active sites^[48]. Therefore, the microstructure evolution of electrocatalysts should be considered in the future catalyst design.

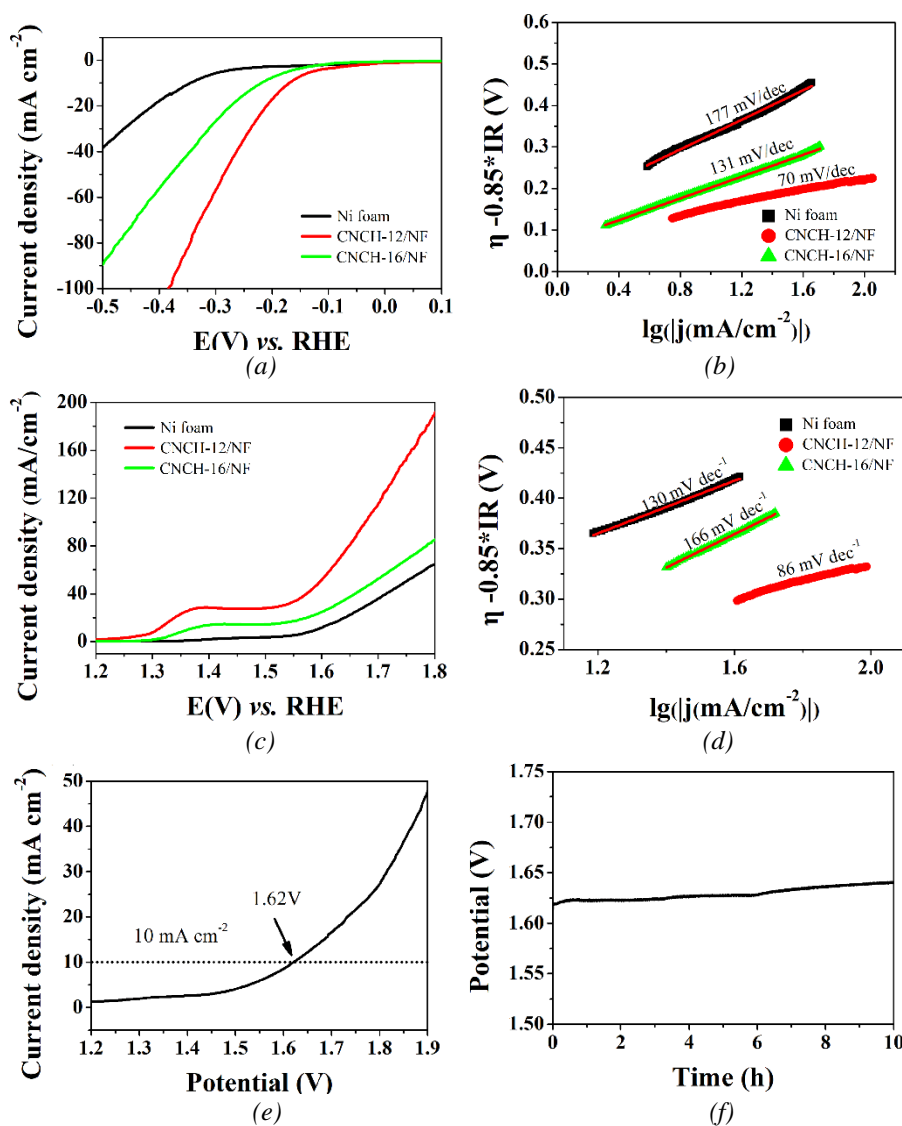


Fig. 4. The LSV curves measured at 5 mV s^{-1} in 1 M KOH solution for HER without iR compensation (a) and the corresponding Tafel plots (b); the LSV curves measured at 5 mV s^{-1} in 1 M KOH solution for OER without iR compensation (c) and the corresponding Tafel plots (d); the LSV curve in a two-electrode system using CNCH-12/NF as cathodic and anodic electrodes (e) and its long-term stability test carried out under a constant current density of 10 mA cm^{-2} (f).

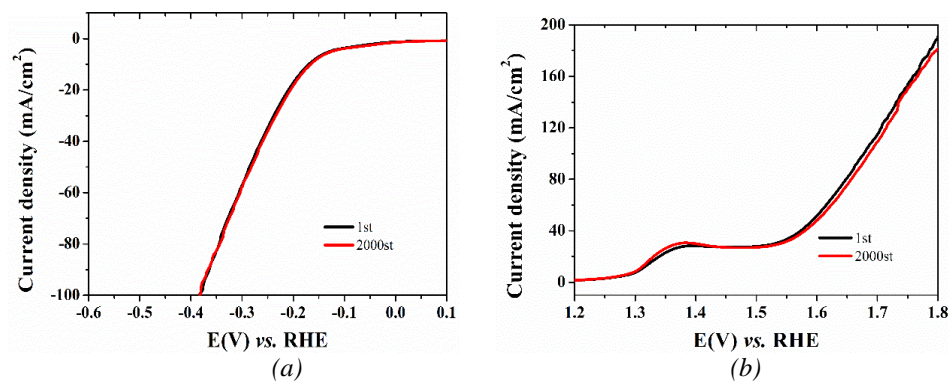


Fig. 5. The LSV curves of CNCH-12/NF for HER (a) and OER (b) after 2000 cyclic voltammetry cycles.

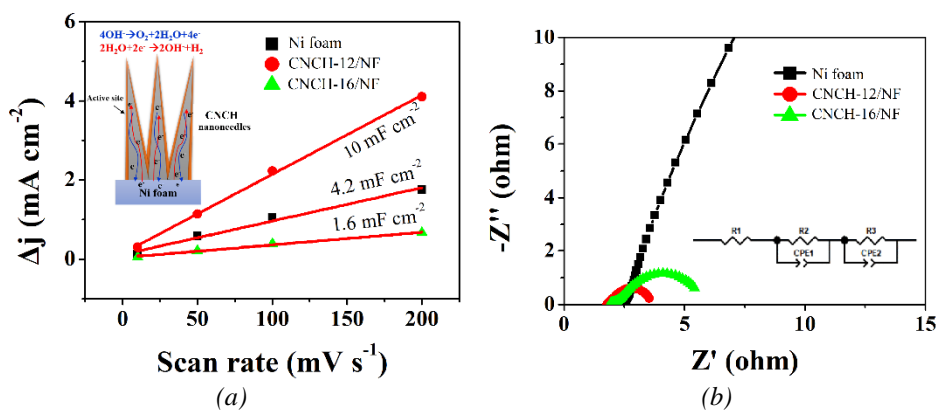


Fig. 6. (a) Estimation of C_{dl} by plotting the current density against scan rate to fit a linear regression. (b) Nyquist plots at 0.5V (vs SCE) from 10 kHz to 0.01 Hz with an amplitude of 5 mV.

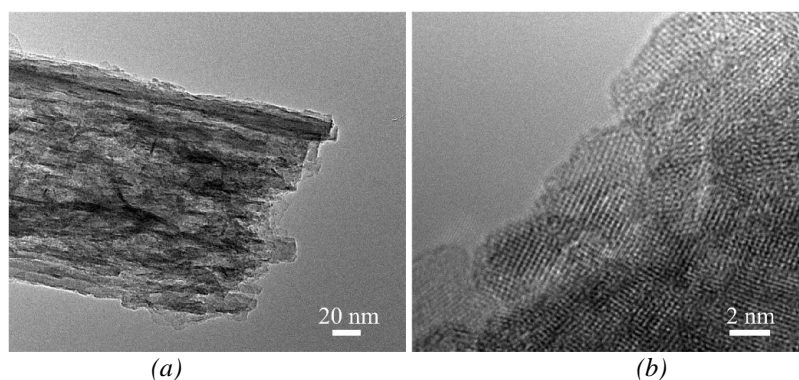


Fig. 7. TEM images of CNCH-12/NF after electrochemical measurement.

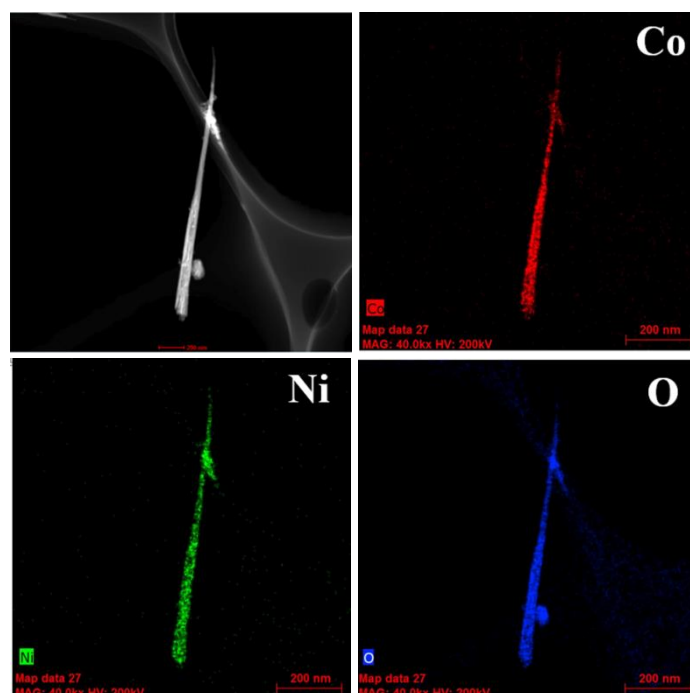


Fig. 8. EDX elemental mapping images of CNCH-12/NF after electrochemical test.

4. Conclusions

In summary, we perform a facile hydrothermal method to synthesis CNCH nanoneedles self-supported on Ni foam. Such materials show 1D nanoneedles with hybrid amorphous/crystalline structures, which enable more active sites, better charge transport and mass transfer. Low overpotentials of 171 mV for HER at 10 mA cm^{-2} and 368 mV for OER at 50 mA cm^{-2} were achieved in 1 M KOH solution, together with excellent full water-splitting performance, achieving the current density of 10 mA cm^{-2} at 1.62V.

Acknowledgements

The authors would like to acknowledge funding from the National Natural Science Foundation of China (11572057, 11832007, 51702027), China Postdoctoral Science Foundation (2018M631082) and Applied Basic Research Program of Sichuan Province (2019YJ0668).

References

- [1] J. A. Turner, *Science* **305**(5686), 972 (2004).
- [2] M. I. Hoffert et al., *Science* **298**(5595), 981 (2002).
- [3] X. Wang et al., *Advanced Energy Materials* **2**(1), 42 (2012).
- [4] N.-T. Suen et al., *Chemical Society Reviews* **46**(2), 337 (2017).
- [5] Y. Liu et al., *Chem* **4**(6), 1263 (2018).
- [6] Z. Tang et al., *Angewandte Chemie International Edition* **49**(27), 4603 (2010).
- [7] C. Zhu et al., *Chemical Society Reviews* **47**(12), 4332 (2018).
- [8] Y. P. Zhu et al., *Angewandte Chemie International Edition* **56**(5), 1324 (2017).
- [9] W. Lei et al., *International Journal of Hydrogen Energy* **41**(45), 20515 (2016).

- [10] E. Hu et al., *Energy & Environmental Science* **11**(4), 872 (2018).
- [11] J. Wan et al., *Advanced Functional Materials* **27**(45), 1703933 (2017).
- [12] H. Zhou et al., *Energy & Environmental Science* **10**(6), 1487 (2017).
- [13] G. Wang et al., *Electrochimica Acta* **247**, 722 (2017).
- [14] L. Yu et al., *Angewandte Chemie International Edition* **57**(1), 172 (2018).
- [15] Y. Jing, Z. Zhou, *ACS Catalysis* **5**(7), 4309 (2015).
- [16] S. Park et al., *Energy & Environmental Science* **5**(11), 9331 (2012).
- [17] T. Reier et al., *ACS Catalysis* **2**(8), 1765 (2012).
- [18] A. Eftekhari, *Materials Today Energy* **5**, 37 (2017).
- [19] R. Frydendal et al., *ChemElectroChem* **1**(12), 2075 (2014).
- [20] L.-L. Feng et al., *Journal of the American Chemical Society* **137**(44), 14023 (2015).
- [21] B. You et al., *Angewandte Chemie International Edition* **55**(34), 9913 (2016).
- [22] B. You et al., *ACS Catalysis* **6**(2), 714 (2016).
- [23] M. Asnavandi et al., *ACS Energy Letters* **3**(7), 1515 (2018).
- [24] J. Liu et al., *ACS Catalysis* **8**(7), 6707 (2018).
- [25] L. Han et al., *Advanced Materials* **28**(23), 4601 (2016).
- [26] R. Xiang et al., *Chinese Journal of Catalysis* **39**(11), 1736 (2018).
- [27] J. Liu et al., *Chemical Communications* **54**(5), 463 (2018).
- [28] H. G. Yang et al., *Nature* **453**(7195), 638 (2008).
- [29] Y. Wang et al., *Chemical Communications* **50**(98), 15529 (2014).
- [30] M. Xie et al., *Nanoscale* **9**(43), 16612 (2017).
- [31] Y. Q. Jin et al., *Journal of Power Sources* **402**, 388 (2018).
- [32] Y. Li et al., *ACS Catalysis* **8**(3), 1913 (2018).
- [33] J. Zhao et al., *Chemical Communications* **54**(39), 4987 (2018).
- [34] J. Wang et al., *Advanced Materials* **29**(14), 1605838 (2017).
- [35] Y. Zheng et al., *Angewandte Chemie International Edition* **57**(26), 7568 (2018).
- [36] Y. Zheng et al., *ACS Nano* **8**(5), 5290 (2014).
- [37] X. Liu et al., *Chemistry of Materials* **26**(5), 1889 (2014).
- [38] A. Sivanantham et al., *Advanced Functional Materials* **26**(26), 4661 (2016).
- [39] J. Huang et al., *Advanced Materials* **30**(39), 1803367 (2018).
- [40] L. Xu et al., *ACS Applied Energy Materials* **1**(3), 1210 (2018).
- [41] W. Liu et al., *Dalton Transactions* **46**(26), 8372 (2017).
- [42] T. Zhang et al., *Nano Energy* **43**, 103 (2018).
- [43] X. Yu et al., *Advanced Energy Materials* **8**(34), 1802445 (2018).
- [44] H. Lin et al., *ChemSusChem* **10**(12), 2597 (2017).
- [45] B. Lu et al., *International Journal of Hydrogen Energy* **36**(1), 72 (2011).
- [46] X. Lu, C. Zhao, *Nature Communications* **6**, 6616 (2015).
- [47] Y. Wang et al., *Advanced Functional Materials* **28**(4), 1703363 (2018).
- [48] H. Zhou et al., *Energy & Environmental Science* **11**(10), 2858 (2018).